

CHEMICAL PHYSICS

Observation of the fastest chemical processes in the radiolysis of water

Z.-H. Loh^{1*}, G. Doumy², C. Arnold^{3,4,5}, L. Kjellsson^{6,7}, S. H. Southworth², A. Al Haddad², Y. Kumagai², M.-F. Tu², P. J. Ho², A. M. March², R. D. Schaller^{8,9}, M. S. Bin Mohd Yusof¹, T. Debnath¹, M. Simon¹⁰, R. Welsch^{3,5}, L. Inhester³, K. Khalil¹¹, K. Nanda¹², A. I. Krylov^{3,12}, S. Moeller¹³, G. Coslovich¹³, J. Koralek¹³, M. P. Minitti¹³, W. F. Schlotter¹³, J.-E. Rubensson⁶, R. Santra^{3,4,5*}, L. Young^{2,14*}

Elementary processes associated with ionization of liquid water provide a framework for understanding radiation-matter interactions in chemistry and biology. Although numerous studies have been conducted on the dynamics of the hydrated electron, its partner arising from ionization of liquid water, H_2O^+ , remains elusive. We used tunable femtosecond soft x-ray pulses from an x-ray free electron laser to reveal the dynamics of the valence hole created by strong-field ionization and to track the primary proton transfer reaction giving rise to the formation of OH. The isolated resonance associated with the valence hole ($\text{H}_2\text{O}^+/\text{OH}$) enabled straightforward detection. Molecular dynamics simulations revealed that the x-ray spectra are sensitive to structural dynamics at the ionization site. We found signatures of hydrated-electron dynamics in the x-ray spectrum.

Radiolysis of liquid water is a universal phenomenon that accompanies the interaction of high-energy radiation with matter in aqueous environments. It is of fundamental importance in many domains (1), including water-cooled nuclear reactors where radiolysis products cause corrosion (2). Living organisms consist of 80% water by weight (3); hence, the detection of radiation-induced genomic damage via radiolysis of water is foundational to medical treatment, diagnosis, and even extended human space flight (4).

Although ionizing radiation is delivered via various vehicles (x-rays, γ -rays, charged particles), its interaction with matter can be understood conceptually as individual absorption events along the particle path accompanied by a cascade of electrons, ions, and radicals (5). Consider the most elementary process: ionization of pure liquid water, which leads to the formation of a hydrated-electron precursor and a cationic hole (H_2O^+). Both spe-

cies are very reactive. The dynamics of the hydrated electron, e_{aq}^- , has been the subject of numerous studies (6–11) since the discovery of its visible spectrum (12), which peaks at 718 nm and spans 500 to 1000 nm, a range convenient for ultrafast laser spectroscopies. In stark contrast, its ionization partner, H_2O^+ , has not been experimentally detected. The H_2O^+ is predicted to undergo rapid sub-100-fs proton transfer to a neighboring water molecule to yield the hydronium cation (H_3O^+) and the hydroxyl radical (OH) (1, 13, 14). Attempts to directly observe the H_2O^+ cation using ultrafast visible or ultraviolet probes have been inconclusive because of its ultrashort lifetime and masked spectral signature (6, 14, 15). Thus, basic questions regarding the ionization of water remain. What is the lifetime of H_2O^+ ? What are the absorption spectra of H_2O^+ and OH? What is the extent of hole delocalization in H_2O^+ and its time scale for localization relative to proton transfer?

Here, we introduce an ultrafast x-ray probe that enables us to track the primary chemical reaction following ionization of liquid water, namely $\text{H}_2\text{O}^+ + \text{H}_2\text{O} \rightarrow \text{OH} + \text{H}_3\text{O}^+$. Combined experiment and theory yield insight for this newly accessible spectral regime. X-rays are well suited for probing the short-lived H_2O^+ cation and OH radical, as their absorption lines fall cleanly in the water window. Removal of an electron from the outermost valence orbital (1b_1) of H_2O produces a new transition for H_2O^+ that is red-shifted from the $1\text{a}_1 \rightarrow 4\text{a}_1$ pre-edge transition at 535 eV (16) roughly by the highest occupied molecular orbital–lowest unoccupied molecular orbital (HOMO-LUMO) gap ΔE (17), as shown in Fig. 1A. The OH radical, isoelectronic to H_2O^+ , possesses a nearby x-ray absorption resonance, whereas the other product of proton transfer, H_3O^+ , has resonances that fall in a region of strong water

absorption (Fig. 1B). Figure 1C shows the experimental configuration, consisting of a 60-fs, 800-nm strong-field ionization pump (10), a tunable ~30-fs ultrafast x-ray probe from the Linac Coherent Light Source (LCLS) x-ray free electron laser (XFEL) (18), and three photon-in/photon-out detection channels.

Signatures of the impulsively produced valence hole and excess electron appeared in all three detection channels when the incident x-ray energy was scanned. Figure 2A displays data from the dispersed fluorescence channel, whereas the transmission mode is used in Fig. 2, B to D. Figure 2A shows absorption before and after ionization ($\Delta t < 0$ ps and $\Delta t > 100$ fs, respectively). At negative time delay, the absorption is that of liquid water—that is, nonresonant ionization of the valence and inner-valence levels of water plus the pre-edge transition. (Saturation effects prevented a clear observation of the pre-edge resonance.) At positive time delay, two new features are apparent: an absorption resonance at 525.9 eV and a shift of the pre-edge absorption to lower energies. The new absorption resonance is consistent with the creation of a hole in the outermost valence level of liquid water. The corresponding H_2O^+ transition energy can be estimated to be 526.9 eV using the binding energies in liquid water of the O 1s core level (538.1 eV) (19) and the 1b_1 HOMO (11.2 eV) (20). The isoelectronic OH exhibits a gas-phase absorption peak at 525.85 eV (21).

The H_2O^+ cation produced by the ionization of liquid water is widely expected to decay via a pseudo-first-order reaction involving proton transfer to a neighboring water molecule,



to yield the OH radical and the H_3O^+ species. In the absence of electron scavengers, the OH radical subsequently undergoes geminate recombination (22) with the ejected electron to give OH^- . The time-resolved differential absorption spectrum, $\Delta A = A(\Delta t) - A(\Delta t < 0)$, showed a prompt increase at time zero, followed by a narrowing of the spectral width within the first picosecond, and finally a gradual decay at longer time delays (Fig. 2B). We modeled this behavior as sequential kinetics: The species initially produced by ionization decays with lifetime τ_1 to give an intermediate species with lifetime τ_2 , with absorption spectra $S_1(E)$ and $S_2(E)$, respectively.

We assigned $S_2(E)$, obtained by averaging ΔA for time delays between 1.5 and 5.8 ps, to the OH radical (Fig. 2C). $S_2(E)$ can be fit to a sum of two Lorentzians: a main peak at 525.97 ± 0.08 eV and a sideband, weaker by a factor of ~7, at 526.45 ± 0.12 eV. The 0.48-eV energy spacing between the two peaks is in reasonable agreement with the 0.53-eV spacing of the vibrational progression for core-excited

¹Division of Chemistry and Biological Chemistry, School of Physical and Mathematical Sciences, Nanyang Technological University, Singapore. ²Chemical Sciences and Engineering Division, Argonne National Laboratory, Lemont, IL, USA. ³Center for Free-Electron Laser Science, DESY, Hamburg, Germany. ⁴Department of Physics, Universität Hamburg, Hamburg, Germany. ⁵Hamburg Centre for Ultrafast Imaging, Hamburg, Germany. ⁶Department of Physics and Astronomy, Uppsala University, Uppsala, Sweden. ⁷European XFEL GmbH, Schenefeld, Germany. ⁸Center for Nanoscale Materials, Argonne National Laboratory, Lemont, IL, USA. ⁹Department of Chemistry, Northwestern University, Evanston, IL, USA. ¹⁰Sorbonne Université and CNRS, Laboratoire de Chimie Physique-Matière et Rayonnement, LCPMR, F-750005 Paris, France. ¹¹Department of Energy Conversion and Storage, Technical University of Denmark, Roskilde, Denmark. ¹²Department of Chemistry, University of Southern California, Los Angeles, CA, USA. ¹³Linac Coherent Light Source, SLAC National Accelerator Laboratory, Menlo Park, CA, USA. ¹⁴Department of Physics and James Franck Institute, University of Chicago, Chicago, IL, USA.

*Corresponding author. Email: zhiheng@ntu.edu.sg (Z.-H.L.); robin.santra@cfdl.de (R.S.); young@anl.gov (L.Y.)

gas-phase OH (21). Both peaks have a common FWHM (full width at half maximum) of 0.48 ± 0.02 eV, considerably broader than the 0.1-eV spectral bandwidth of the XFEL pulses and the 0.147-eV natural linewidth (21), which suggests inhomogeneous broadening by the solvent environment.

With the x-ray absorption line shape of the aqueous OH radical $S_2(E)$ determined, the next step is to extract the time constants τ_1 and τ_2 and the spectral line shape of the short-lived component $S_1(E)$. We used a Gaussian instrument response function of 106-fs FWHM and performed a surface fit of the experimental data shown in Fig. 2B. (We did not convolve the kinetic model with the experimental energy resolution of 0.1-eV FWHM because the experimentally observed spectral features were much broader.) The surface fit yielded $\tau_1 = 0.18 \pm 0.02$ ps, $\tau_2 = 14.2 \pm 0.4$ ps, and a Lorentzian absorption line shape $S_1(E)$ centered at 526.01 ± 0.13 eV with a FWHM of 0.98 ± 0.04 eV. The decay of the OH radical, τ_2 , most likely originates from geminate recombination of the OH radical with a hydrated electron. The recombination time constant of 14.2 ± 0.4 ps is considerably shorter than those reported in the literature (22), most likely because of the high initial ionization fraction accelerating the geminate recombination process. Geminate recombination between e_{aq}^- and OH in ionized liquid water has been extensively investigated by time-resolved optical spectroscopy (22) and is beyond the scope of the present study. Nonetheless, considering the relative diffusion coefficients of the reactants and the reaction radius, our observed time scale for geminate recombination suggests an approximate ionization fraction of 1.7%, in relatively good agreement with the ionization fraction estimated on the basis of OH x-ray absorbance (see below). The spectral line shape $S_1(E)$ and time constant τ_1 can be assigned either to the decay of H_2O^+ or to the cooling of a vibrationally hot OH radical. Both species should exhibit a larger spectral linewidth than the OH radical. The x-ray absorption linewidth of H_2O^+ may be similar to the 1.5 eV-wide $1b_1$ band in the valence photoelectron (20) and the x-ray emission spectra (23) of liquid water, whose widths have been attributed to a multitude of hydrogen-bonding configurations and intermolecular geometries. The x-ray absorption spectrum of vibrationally excited OH may be broadened if additional hot-band transitions are present.

Further insight into the early-time dynamics was obtained with time traces at three selected photon energies: 525.43, 525.93, and 526.73 eV (Fig. 2D). These time traces correspond to the isotropic signal $\Delta A_{iso} = (\Delta A_{||} + 2\Delta A_{\perp})/3$, reconstructed from measurements in which the relative polarizations of the pump and probe pulses are parallel ($\Delta A_{||}$) and perpendicular

(ΔA_{\perp}). ΔA_{iso} is independent of rotational re-orientation of the transient species in solution and is therefore sensitive only to population dynamics. Upon inspection, the ΔA_{iso} time trace for 525.93 eV shows a markedly delayed rise relative to those for 525.43 and 526.73 eV. Attempts to perform a global fit with two time constants could not reproduce the early-time dynamics (see supplementary materials). The presence of this delayed rise suggests the existence of an additional ultrafast process (24) that was not captured in our analysis of the two-dimensional dataset shown in Fig. 2B. Indeed, global fitting of the ΔA_{iso} time traces revealed a new component with a time constant of 46 ± 10 fs, whereas the other two time constants extracted from the fit, 0.16 ± 0.03 ps and 9.2 ± 1.3 ps, are comparable to those obtained from the analysis of the dataset shown in Fig. 2B. This additional time constant appeared as a growth component at 525.93 eV and, to a smaller extent, at 526.73 eV

as well, hence accounting for their delayed appearances relative to the signal at 525.43 eV, which rose with the instrument response function (where prompt absorption by vertically ionized water is expected from the calculated relative positions of the OH and H_2O^+ resonances). That the 46-fs component manifested itself as a growing signal at 525.93 eV, near the peak position of the OH radical absorption maximum at 525.97 eV, strongly suggests that it reflects the time scale for the formation of the OH radical. Given that OH is formed from the decay of the H_2O^+ radical cation, this interpretation would therefore suggest a lifetime of 46 fs for the H_2O^+ radical cation. The experiments were conducted at near-ambient temperature, making them practically relevant. In this non-equilibrium situation, any local temperature rise does not affect the ultrafast proton transfer time scale.

To understand the observed ultrafast dynamics, we performed quantum mechanical

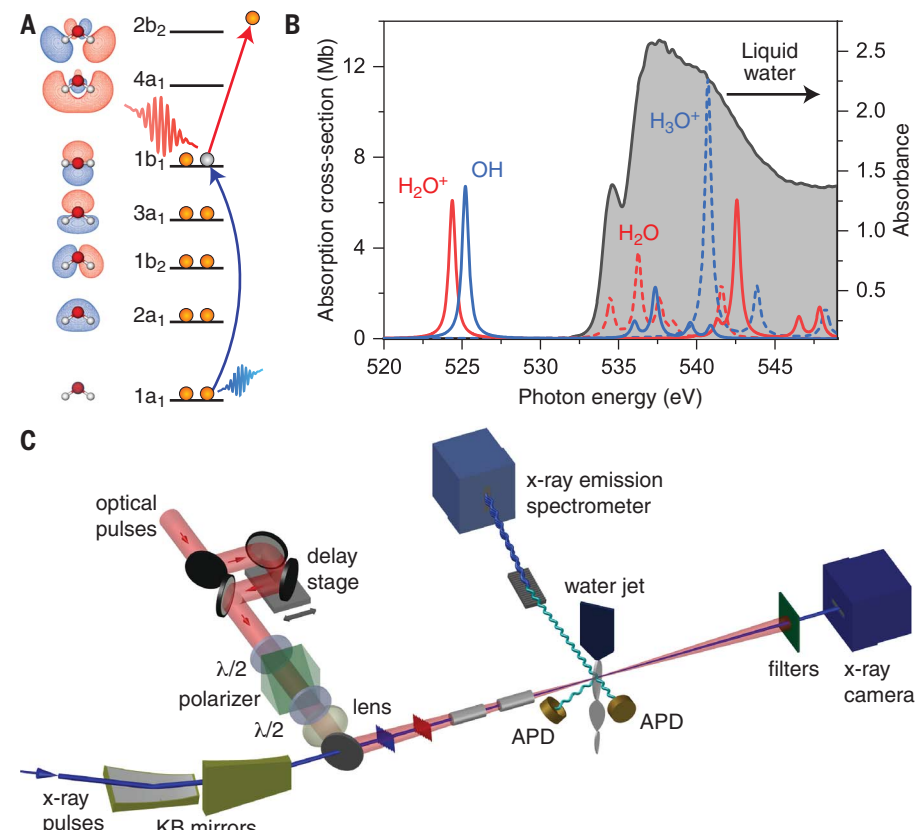


Fig. 1. Ultrafast x-ray laser probe of ionization dynamics of liquid water. (A) Ionization of H_2O produces H_2O^+ with a strong isolated soft x-ray absorption resonance ($1a_1 \rightarrow 1b_1$). (B) Absorption resonances in the gas phase for the four species associated with elementary proton transfer: $H_2O^+ + H_2O \rightarrow OH + H_3O^+$ calculated with 6-311(2+,+)G(2df,p) basis with uncontracted core (oxygen) using fc-cvqs-EOM-CCSD (36). Only H_2O^+ and OH fall outside the region of strong absorption by liquid water (37) (i.e., in the water window). (C) Schematic of the experimental setup: 800-nm strong-field ionization pump and time-delayed x-ray probe. The x-ray probe is monitored simultaneously in transmission, total fluorescence and dispersed fluorescence as a function of pump-probe time delay and incident photon energy (see supplementary materials).

and classical (QM/MM) excited-state molecular dynamics simulations of liquid water following strong-field ionization. We considered initial ionization in the upper 1.5 eV of the valence band and averaged across 107 initial geometries of liquid water. Non-Born-Oppenheimer effects were taken into account by Tully's fewest-switches surface-hopping approach (25). We combined a QM description of a $(\text{H}_2\text{O})_{12}^+$ cluster with an MM description of surrounding water molecules. The electronic structure was obtained at the Hartree-Fock level of theory using Koopmans' theorem to obtain singly ionized states and using the 6-31G basis set as implemented in our software package XMOLCULE (26, 27) (see supplementary materials).

Our simulations explored to what extent transient x-ray absorption is sensitive to ultrafast structural dynamics in water. The time-resolved x-ray absorption spectrum of the valence hole is shown in Fig. 3A for the first 100 fs after the initial hole formation. Although initially electronic states down to HOMO-6 were populated, the trajectories arrived at the cationic ground state within 25 fs (Fig. 3B) and non-Born-Oppenheimer effects were no longer present. This was accompanied by hole localization on a comparable time scale.

Proton transfer can be characterized by the distance between the charge and hole center. Directly after ionization, the charge and hole are overlapped at the H_2O^+ ; as proton transfer proceeds, the hole stays on the OH moiety, while the charge is carried away by the H_3O^+ (14). Figure 3C shows that the charge-hole separation is correlated with the completion of proton transfer. Within our model using bond-order analysis (28), the proton transfer time scale was found to be 60 fs, in good agreement with (14). We further investigated the chemical environment surrounding the $\text{H}_2\text{O}^+/\text{OH}$, where the valence hole is located, to extract correlations with x-ray spectral signatures. The average distance from the $\text{H}_2\text{O}^+/\text{OH}$ oxygen to the nearest H_2O oxygen is shown in Fig. 3D along with the spectral shift (the peak position of Fig. 3A). Initially, the partially negatively charged oxygens are pulled toward the region of positive charge (H_2O^+), giving rise to the redshift of the absorption peak. This motion initiates proton transfer; thus, at the point of maximum redshift, proton transfer is only about 25% complete (Fig. 3C). As a consequence of charge-hole separation, the distance between OH and the neighboring oxygens increases, and the redshift shrinks. In this way, proton transfer is indirectly reflected in the time evolution of the x-ray absorption peak position.

The results presented here offer insight into the elementary dynamics of the highly reactive and short-lived ion and neutral radical species in ionized liquid water. Our experimental

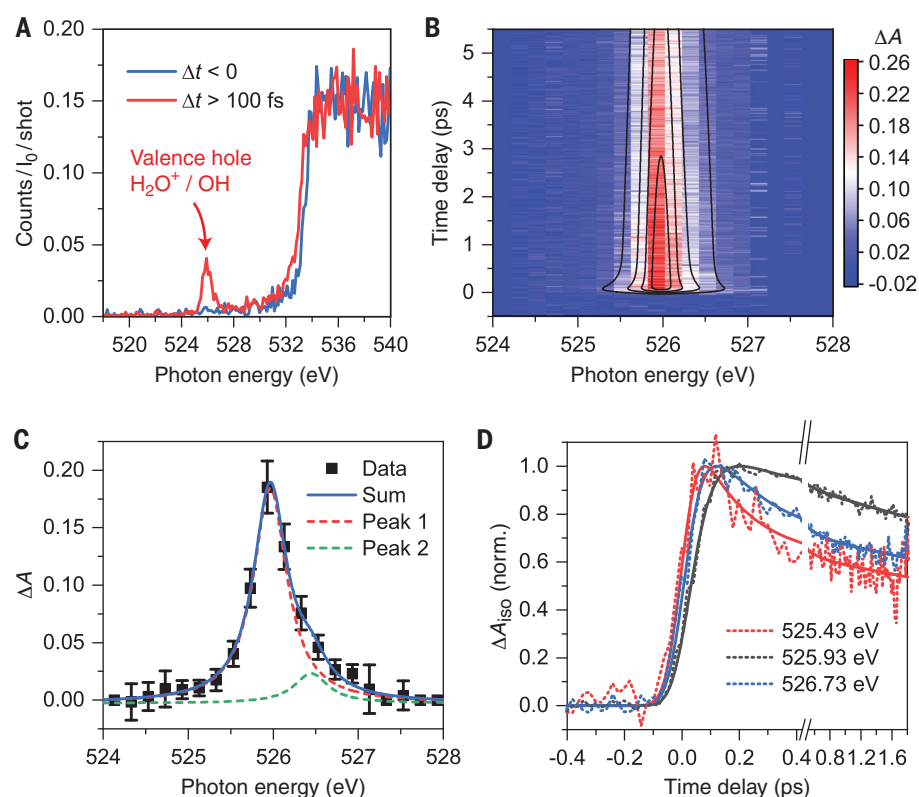


Fig. 2. Transient x-ray absorption spectroscopy for the reaction $\text{H}_2\text{O}^+ + \text{H}_2\text{O} \rightarrow \text{OH} + \text{H}_3\text{O}^+$.

(A) Absorption for $\Delta t < 0$ and $\Delta t > 100$ fs monitored through the dispersed fluorescence channel. (B) Differential absorption ΔA in the valence hole ($\text{H}_2\text{O}^+/\text{OH}$) region. Spectra collected at 216 time delays between 1.5 and 5.8 ps are averaged to produce the resonance profile, which is fit to a sum of two Lorentzians. Error bars denote SD. A total of 31 energy sweeps and 27,546 shots are collected. (C) X-ray absorption spectrum of the aqueous OH radical. (D) Polarization averaged time traces at three x-ray probe energies: 525.43, 525.93, and 526.73 eV.

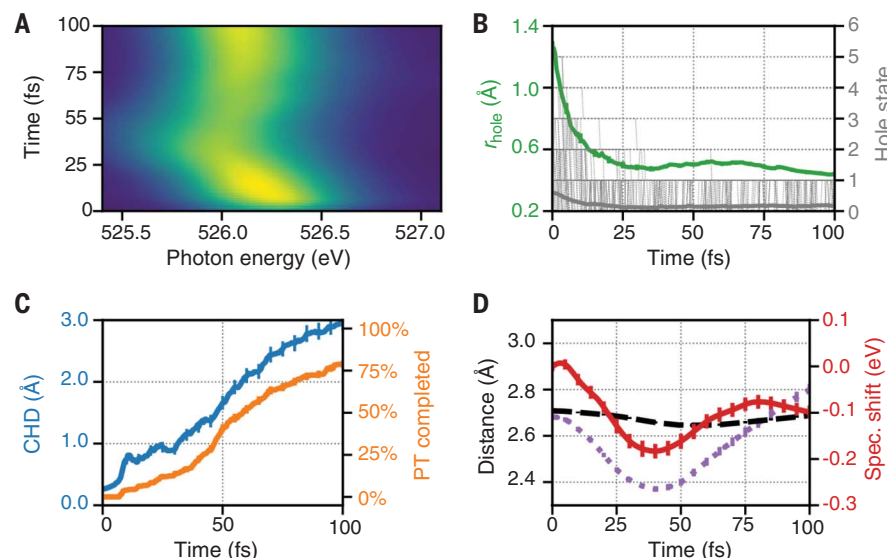


Fig. 3. Calculated x-ray absorption spectra and trajectory analysis. (A) Resonant x-ray absorption spectrum of ionized water. (B) Hole radius (green) and nonadiabatic dynamics (gray, solid line shows average). (C) Charge-hole distance (CHD) (blue) and completed proton transfer percentage (orange). (D) Average distance between oxygens in H_2O molecules (black) along with the average distance of the $\text{H}_2\text{O}^+/\text{OH}$ oxygen to the nearest oxygen (purple) and the spectral shift of the x-ray absorption resonance (red).

approach offers several advantages over previous attempts (6, 14, 15) to determine the lifetime of the elusive H_2O^+ radical cation. First, relative to traditional two-photon ultraviolet photoionization, strong-field ionization provides access to a large concentration of ionized species in solution. Assuming a cross section of ~ 7 Mbarn for the O 1s resonant absorption of the OH radical, we estimated an ionization fraction of $\sim 0.8\%$ under our experimental conditions. Second, the H_2O^+ and OH radicals exhibit strong O 1s \rightarrow 2p-like resonant transitions in the soft x-ray absorption spectra because they possess open O 2p subshells. These resonances occur in the background-free, near-edge spectral region, enabling detection down to concentrations of a few millimolar. In comparison, previous attempts using spectrally resolved visible transient absorption spectroscopy to observe the H_2O^+ radical cation via its predicted absorption signature at 2.3 eV were unsuccessful because its weak absorption was masked by the strong, broad hydrated-electron absorption feature and further complicated by cross-phase modulation artifacts (6, 14, 15).

Our study revealed three distinct time scales in the early-time dynamics of ionized liquid water: 46 ± 10 fs, 0.18 ± 0.02 ps, and 14.2 ± 0.4 ps, tentatively assigned to the decay of the H_2O^+ radical cation via proton transfer, vibrational cooling of the hot OH radical produced from H_2O^+ , and geminate recombination of OH with the hydrated-electron by-product, respectively. The first two processes, hitherto unobserved, are of particular interest. The assignment of the 46-fs component to the lifetime of the H_2O^+ cation is supported by QM/MM molecular dynamics simulations, which predict a lifetime of 60 fs. However, we note that the same simulations also showed that hole localization occurs within 30 fs. As such, with the currently available time resolution, hole localization also contributed to the observed dynamics. On the intermediate time scale, the 0.18-ps component was tentatively assigned to vibrational cooling of hot OH radicals that are produced upon ultrafast proton transfer. The formation of a vibrationally excited OH product from H_2O^+ is likely, considering the 3% change in equilibrium OH bond lengths between gas-phase H_2O^+ (0.9992 Å) (29) and OH (0.9697 Å) (30). The assignment of the 0.18-ps component to vibrational relaxation of the OH radical is supported by studies of the OH stretch of liquid H_2O , where numerous time-resolved infrared spectroscopic measurements show vibrational relaxation and vibrational energy transfer occurring within 0.2 to 0.3 ps (31, 32).

We expect that a future study with higher time resolution and signal-to-noise ratios could furnish a more accurate H_2O^+ lifetime and at the same time permit the observation

of ultrafast dynamics involving possible hole alignment, coherences, and nonadiabatic dynamics induced by radiolysis. With improved statistics over a wide range of probe photon energies, we also anticipate the possibility of isolating the spectral signatures of H_2O^+ and the hot OH radical. Interestingly, in addition to valence hole dynamics observed at 526 eV, the soft x-ray probe appeared to be sensitive to the dynamics of the electron that was injected into the solvent by ionization. The spectral changes observed in the vicinity of the pre-edge absorption (531.0 to 533.7 eV) fit a universal time constant of 0.26 ± 0.03 ps that matches previous studies of hydrated-electron formation (7, 8) (see supplementary materials). Future experiments focusing on the pre-edges and main edges of ionized liquid water that require a sub-micrometer-thick liquid jet could potentially yield the electronic energy level diagram of ionized liquid water (33) and shed light on its electronic relaxation dynamics, as well as possibly discern the cavity versus noncavity model for the structure of the hydrated electron (34).

REFERENCES AND NOTES

- B. C. Garrett *et al.*, *Chem. Rev.* **105**, 355–390 (2005).
- S. Gordon, in *Early Developments in Radiation Chemistry*, J. Kroh, Ed. (Royal Society of Chemistry, 1989), pp. 163–204.
- E. Alizadeh, L. Sanche, *Chem. Rev.* **112**, 5578–5602 (2012).
- F. E. Garrett-Bakelman *et al.*, *Science* **364**, eaau8650 (2019).
- M. Inokuti, *Rev. Mod. Phys.* **43**, 297–347 (1971).
- F. H. Long, H. Lu, K. B. Eisenthal, *Phys. Rev. Lett.* **64**, 1469–1472 (1990).
- A. Migu, Y. Gauduel, J. L. Martin, A. Antonetti, *Phys. Rev. Lett.* **58**, 1559–1562 (1987).
- P. Kambhampati, D. H. Son, T. W. Kee, P. F. Barbara, *J. Phys. Chem. A* **106**, 2374–2378 (2002).
- M. H. Elkins, H. L. Williams, A. T. Shreve, D. M. Neumark, *Science* **342**, 1496–1499 (2013).
- J. Li, Z. Nie, Y. Y. Zheng, S. Dong, Z.-H. Loh, *J. Phys. Chem. Lett.* **4**, 3698–3703 (2013).
- J. M. Herbert, M. P. Coons, *Annu. Rev. Phys. Chem.* **68**, 447–472 (2017).
- E. J. Hart, J. W. Boag, *J. Am. Chem. Soc.* **84**, 4090–4095 (1962).
- E. Kamarchik, O. Kostko, J. M. Bowman, M. Ahmed, A. I. Krylov, *J. Chem. Phys.* **132**, 194311 (2010).
- O. Marsalek *et al.*, *J. Chem. Phys.* **135**, 224510 (2011).
- Y. Gauduel, S. Pommere, A. Migu, A. Antonetti, *Chem. Phys.* **149**, 1–10 (1990).
- T. Fransson *et al.*, *Chem. Rev.* **116**, 7551–7569 (2016).
- C. G. Elles, C. A. Rivera, Y. Zhang, P. A. Pieniazek, S. E. Bradforth, *J. Chem. Phys.* **130**, 084501 (2009).
- P. Emma *et al.*, *Nat. Photonics* **4**, 641–647 (2010).
- B. Winter, E. F. Aziz, U. Hergenhahn, M. Faubel, I. V. Hertel, *J. Chem. Phys.* **126**, 124504 (2007).
- K. Nishizawa *et al.*, *Phys. Chem. Chem. Phys.* **13**, 413–417 (2011).
- S. Stranges, R. Richter, M. Alagia, *J. Chem. Phys.* **116**, 3676–3680 (2002).
- R. A. Crowell, D. M. Bartels, *J. Phys. Chem.* **100**, 17940–17949 (1996).
- J. H. Guo *et al.*, *Phys. Rev. Lett.* **89**, 137402 (2002).
- M. J. Rosker, M. Dantus, A. H. Zewail, *J. Chem. Phys.* **89**, 6113–6127 (1988).
- J. C. Tully, *J. Chem. Phys.* **93**, 1061–1071 (1990).
- Y. Hao, L. Inhester, K. Hanasaki, S.-K. Son, R. Santra, *Struct. Dyn.* **2**, 041707 (2015).
- K. Khalili *et al.*, *Struct. Dyn.* **6**, 044102 (2019).
- L. Inhester *et al.*, *J. Phys. Chem. Lett.* **9**, 1156–1163 (2018).
- T. R. Huet, C. J. Pursell, W. C. Ho, B. M. Dinelli, T. Oka, *J. Chem. Phys.* **97**, 5977–5987 (1992).
- K. P. Huber, G. Herzberg, in *NIST Chemistry WebBook, NIST Standard Reference Database Number 69*, P. J. Linstrom, W. G. Mallard, Eds. (National Institute of Standards and Technology); <http://webbook.nist.gov>.
- F. Perakis *et al.*, *Chem. Rev.* **116**, 7590–7607 (2016).
- M. L. Cowan *et al.*, *Nature* **434**, 199–202 (2005).
- A. P. Gaiduk, T. A. Pham, M. Govoni, F. Paesani, G. Galli, *Nat. Commun.* **9**, 247 (2018).
- R. E. Larsen, W. J. Glover, B. J. Schwartz, *Science* **329**, 65–69 (2010).
- L. Young, Z.-H. Loh, R. Santra, C. Arnold, Data for “Observation of the fastest chemical processes in the radiolysis of water.” Zenodo repository, DOI: 10.5281/zenodo.3543680.
- M. L. Vidal, X. Feng, E. Epifanovsky, A. I. Krylov, S. Coriani, *J. Chem. Theory Comput.* **15**, 3117–3133 (2019).
- M. Nagasaka, T. Hatsui, T. Horigome, Y. Hamamura, N. Kosugi, *J. Electron Spectrosc. Relat. Phenom.* **177**, 130–134 (2010).

ACKNOWLEDGMENTS

Funding: Supported by the U.S. Department of Energy (DOE) Office of Science, Office of Basic Energy Sciences, Chemical Sciences, Geosciences, and Biosciences Division, which supports the Argonne group under contract DE-AC02-06CH11357. Use of the LCLS, SLAC National Accelerator Laboratory, and resources of the Center for Nanoscale Materials, Argonne National Laboratory, are supported by DOE Office of Science, Office of Basic Energy Sciences under contracts DE-AC02-76SF00515 and DE-AC02-06CH11357. Also supported by Laboratory Directed Research and Development funding from Argonne National Laboratory for conceptual design and proposal preparation (L.Y.); Singapore Ministry of Education grants MOE2014-T2-2-052 and RG105/17 (Z.-H.L., M.S.B.M.Y., and T.D.); Swedish Science Council grant 2018-04088 (L.K. and J.-E.R.); the CNRS GotoXFEL program (M.S.); the Deutsche Forschungsgemeinschaft Cluster of Excellence “Advanced Imaging of Matter” (EXC 2056, project ID 390715994) (C.A., R.W., and R.S.); DOE Office of Science, Office of Basic Energy Sciences, Chemical Sciences, Geosciences, and Biosciences Division grant DE-SC0019451 (L.I. and R.S.); the European Research Council under the European Union’s Horizon 2020 research and innovation program (grant agreement 681881) (K.K.); NSF grant CHE-1856342 (A.I.K. and K.N.); and a Simons Fellowship in Theoretical Physics and Mildred Dresselhaus Award from the Hamburg Centre for Ultrafast Imaging, which supported a sabbatical at DESY in Germany (A.I.K.). **Author contributions:** L.Y., Z.-H.L., and R.S. originated the project concept; W.F.S., G.D., M.-F.T., R.D.S., and S.H.S. designed the experimental apparatus and characterized the target; Z.-H.L., G.D., C.A., L.K., S.H.S., A.A.H., Y.K., M.-F.T., P.J.H., A.M.M., M.S.B.M.Y., T.D., M.S., S.M., G.C., J.K., M.P.M., W.F.S., J.-E.R., and L.Y. executed the experiment and collected the experimental data; Z.-H.L., Y.K., L.K., J.-E.R., and L.Y. analyzed the experimental data; R.S., C.A., R.W., L.I., K.K., N.I.K., and A.I.K. provided supporting theoretical calculations; L.Y., Z.-H.L., R.S., and C.A. wrote the paper with comments from all authors. L.Y. was responsible for the coordination of the project. **Competing interests:** A.I.K. is a board member and a part owner of Q-Chem Inc. **Data and materials availability:** The underlying data are available in the supplementary materials and Zenodo, the CERN repository (35).

SUPPLEMENTARY MATERIALS

science.sciencemag.org/content/367/6474/179/suppl/DC1
Materials and Methods
Supplementary Text
Figs. S1 to S11
Tables S1 to S3
References (38–51)

12 September 2019; accepted 15 November 2019
10.1126/science.aaq4740

Observation of the fastest chemical processes in the radiolysis of water

Z.-H. Loh, G. Doumy, C. Arnold, L. Kjellsson, S. H. Southworth, A. Al Haddad, Y. Kumagai, M.-F. Tu, P. J. Ho, A. M. March, R. D. Schaller, M. S. Bin Mohd Yusof, T. Debnath, M. Simon, R. Welsch, L. Inhester, K. Khalili, K. Nanda, A. I. Krylov, S. Moeller, G. Coslovich, J. Koralek, M. P. Minitti, W. F. Schlotter, J.-E. Rubensson, R. Santra and L. Young

Science 367 (6474), 179-182.
DOI: 10.1126/science.aaz4740

The "hole" story of water ionization

The direct observation of the cationic hole H_2O^+ that is formed in liquid water after ionization has been a long-standing experimental challenge. Previous attempts using optical and ultraviolet techniques have failed to reveal its key spectroscopic signature during ultrafast transformation into a OH radical. Loh *et al.* address this gap by using intense, ultrafast x-ray pulses from an x-ray free electron laser at ~530 electron volts. They found compelling evidence for the formation H_2O^+ and its decay to an OH radical by a proton transfer mechanism and elucidated the other fastest – time scale steps in the early-time dynamics of ionized liquid water.

Science, this issue p. 179

ARTICLE TOOLS

<http://science.sciencemag.org/content/367/6474/179>

SUPPLEMENTARY MATERIALS

<http://science.sciencemag.org/content/suppl/2020/01/08/367.6474.179.DC1>

REFERENCES

This article cites 48 articles, 3 of which you can access for free
<http://science.sciencemag.org/content/367/6474/179#BIBL>

PERMISSIONS

<http://www.sciencemag.org/help/reprints-and-permissions>

Use of this article is subject to the [Terms of Service](#)

Science (print ISSN 0036-8075; online ISSN 1095-9203) is published by the American Association for the Advancement of Science, 1200 New York Avenue NW, Washington, DC 20005. The title *Science* is a registered trademark of AAAS.

Copyright © 2020 The Authors, some rights reserved; exclusive licensee American Association for the Advancement of Science. No claim to original U.S. Government Works